Journal of Molecular Modeling (2023) 29:63
https://doi.org/10.1007/s00894-023-05462-2

ORIGINAL PAPER

Theoretical insights into the reaction mechanism and kinetics of ampicillin degradation with hydroxyl radical

Seyda Aydogdu[1] · **Arzu Hatipoglu**[1]

Received: 22 December 2022 / Accepted: 23 January 2023 / Published online: 4 February 2023

Abstract

Context Ampicillin (AMP) is a penicillin-class beta-lactam antibiotic widely used to treat infections caused by bacteria. Therefore, due to its widespread use, this antibiotic is found in wastewater, and it contains long-term risks such as toxicity to all living organisms.

Method In this study, the degradation reaction of ampicillin with hydroxyl radical was investigated by the density functional theory (DFT) method. All the calculations were performed with B3LYP functional at 6-31G(d,p) basis set.

Results The thermodynamic energy values and reaction rates of all possible reaction paths were calculated. The addition of the hydroxyl radical to the carbonyl group of the beta-lactam ring is thermodynamically the most probable reaction path. The calculated overall reaction rate constant is 1.36×10^{11} M^{-1} s^{-1}. To determine the effect of temperature on the reaction rate, rate constants were calculated for all reaction paths at five different temperatures. The subsequent reaction kinetics of the most preferred primary route was also examined, and the toxicity values of the intermediates were estimated. The acute toxicity of AMP and its degradation product were calculated using the Ecological Structure Activity Relationships (ECOSAR) software. The degradation product was found to be more toxic than AMP.

Keywords Ampicillin · Hydroxyl radical · DFT · CPCM · Kinetic mechanism

Introduction

Antibiotics are used to prevent and treat diseases in humans and animals [1]. It is known that 90% of antibiotics are distributed to the environment without being metabolized after their use [2]. Therefore, the extensive use of antibiotics has led to their release into the environment, especially the aquatic environment[3]. Antibiotic residues have been detected in aquatic environment samples and even in drinking water [4]. Antibiotic residues play an important role in the occurrence of antibiotic resistance. Their presence in the environment, even in low concentrations, negatively affects both humanity and the ecosystem [5]. It is estimated that only in Europe more than 25,000 people die from antibiotic resistance every year [6]. This is a global problem and also a burden for health systems and needs to be resolved.

Beta-lactam antibiotics are one of the most widely used classes of antibiotics due to their high therapeutic efficacy [7]. Its effectiveness on bacteria is due to its activity of blocking the biosynthetic enzyme responsible for synthesizing the cell wall in bacteria [7, 8]. Ampicillin (AMP) was the first widely prescribed synthetic beta-lactam antibiotic for the treatment of bacterial infections [9]. Due to its widespread use, AMP has been detected up to 27.1 μg L^{-1} even in secondary treated water [5]. The degradability of AMP is a major challenge, and its removal from water by conventional biological methods is often difficult [10]. Advanced oxidation processes (AOPs) used in recent years are promising techniques for the degradation of micropollutants such as beta-lactam antibiotics. [8] In AOPs, highly reactive and short-lived radicals like hydroxyl radical (.OH) are used to mineralize organic contaminants [11].

Although there are many studies on the degradation reactions of AMP in the literature, its kinetics have not been fully explained. These studies are mainly concentrated on increasing degradation rate and finding optimum conditions for designing new catalysts [5, 7, 8, 10, 12–14]. The degradability of AMP can be achieved by different techniques, and the toxicity of the newly formed products is also an important issue [15]. Because the intermediate products formed in the degradation reaction may be more toxic than

✉ Arzu Hatipoglu
hatiparzu@yahoo.com

[1] Department of Chemistry, Yildiz Technical University, 34220 Istanbul, Turkey

the main compound [16], recent literature studies indicate that the aquatic toxicity of AMP to bacteria is increased by the intermediates formed in the degradation reaction [12, 17] . This may be the reason for increasing hydrophilicity for degradation products, and therefore, they can damage the bacterial cell [18].

To combat the disadvantages of the high-level use of AMP, the degradation mechanism needs to be studied in detail. Especially, finding the exact reaction mechanism of AMP is also important in designing appropriate experimental reaction processes and in terms of new antibiotics to be synthesized. The diversity of the mechanisms proposed in experimental studies and the differences in the identified intermediates show that it is not sufficient to investigate the mechanisms and degradation paths of antibiotics only experimentally [4]. Therefore, quantum chemical kinetic studies are very important in this issue. Density functional theory (DFT) methods are more convenient than costly and difficult experimental methods. Studying the degradation mechanism of AMP with DFT methods is a good strategy for assessing the risk associated with the aquatic environment. Although different theoretical models have been developed for the degradation reactions of many different antibiotic molecules [19–21], there is limited quantum chemical information for the AMP + OH reaction in the literature [12].

This study aims to examine the reaction of AMP with OH radical in aqueous media and to determine the most probable reaction path and product distribution. All the reaction path rate constant and thermodynamic stability of the reaction products were determined. The subsequent reaction mechanism was also studied in detail, and the aquatic toxicity of the newly found intermediate was also estimated.

Computational details

All the calculations were carried out at density functional theory (DFT) method using Gaussian 16 program [22]. Optimization and frequency calculations of reactants, pre-reactive complexes, transition state complexes, and products were performed with B3LYP functional at 6-31G(d,p) basis set. All the optimized structures were confirmed by frequency analyses at the same level of the theory. Transition state complexes were characterized by having only one imaginary frequency that belonged to the reaction coordinate, corresponding to a first-order saddle point. IRC calculations were performed to confirm the transition state that connected the true reactants and products [23]. The spin contamination was calculated with basis set superposition effect (BSSE). The spin contamination was found negligible value that did not alter the reaction energy. The solvent effect on the stability and the energy of reactive species was found with the same level of theory in conjunction with the conductor like polarizable continuum model (CPCM) method. The solvent was water with the dielectric constant value of $\varepsilon = 78.355$ [24].

Frontier molecular orbitals (FMO) and molecular electrostatic map (MEP) visualizations were prepared with the GaussView 5.0 program [25]. Natural bond orbital (NBO) analyses were also performed in the Gaussian 16 program. The thermodynamic parameters were calculated by including thermodynamic corrections to the energy at 298.18 K temperature and 1 atm pressure.

Reaction rate constants were calculated by using transition state theory with Wigner correction [26]. The overall rate constant was obtained by summing up the reaction rate constant of each path for the AMP + OH reaction.

$$k_i = K\frac{k_B T}{h} e^{\Delta G^{\#}/RT} \quad (1)$$

where κ is transmission coefficient, k_B is the Boltzmann constant, h is the Plank's constant, T is temperature, and $\Delta G^{\#}$ is the activation free energy.

The half-life time ($t_{1/2}$) of the reaction was calculated by using given equation below,

$$t_{1/2} = \frac{1}{k_{calc}[OH]} \quad (2)$$

in which k_{calc} is the overall rate constant for degradation reaction and [OH] is the concentration of hydroxyl radical in natural waters [27].

The acute toxicity determination of AMP and its degradation product were done by using the Ecological Structure Activity Relationships (ECOSAR) software ECOSAR V2.0 [28–30]. The acute toxicity values were given for green algae, daphnid, and fish as LC_{50} (lethal concentration of tested compound for half of fish and daphnid after 96 h and 46 h respectively) and EC_{50} (effective concentration of a compound for inhibiting the growth half of green algae after 96 h of exposure) values. The toxicities were classified as a globally harmonized system of classification and labelling of chemicals [31].

Results and discussion

Reactant structures and properties

In this study, the kinetics of the reaction mechanism of AMP with OH radical were investigated. Optimized geometric parameters for AMP are given in Table S1 in supporting information. The frontier orbitals energy difference values for reactant molecules are given in Fig. 1. The energy difference between the Highest Occupied Molecular Orbital (HOMO) of AMP and the Lowest Unoccupied

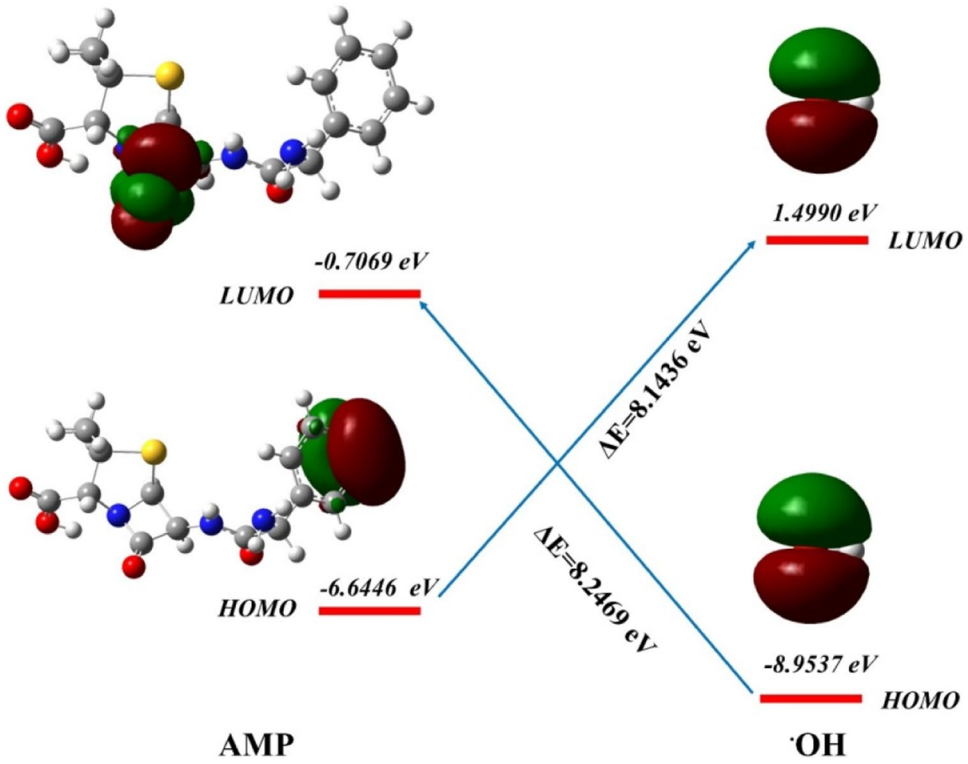

Fig. 1 Frontier molecular orbitals of reactants

Molecular Orbital (LUMO) of OH radical is 8.14 eV, and this value is 0.11 eV smaller than the energy difference of LUMO of AMP to HOMO of OH radical. Thus, the reaction of AMP with OH radical is an orbital controlled reaction [32]. The reaction takes place with a low energy difference from the HOMO of the AMP to the LUMO of the OH radical. It suggests an electrophilic attack of OH to AMP molecule. As seen in Fig. 1, FMOs of the AMP is located on the beta-lactam unit and benzene ring. So, we can deduce that the hydroxyl radical addition to the benzene ring and the carbonyl group of the beta-lactam unit are the possible paths. These results are also consistent with the experimental results [33–35].

Regioselectivity of the reactions is predicted from the frontier molecular orbitals, molecular electrostatic potential graphs, and natural bond orbital analysis. The MEP graph is given in Fig. S1, and NBO results are given in Fig. S2 and Table S2. As seen from the HOMO–LUMO, MEP, and NBO results, it is stereochemically difficult for the hydroxyl radical to approach the hydrogen atoms in the beta-lactam ring of AMP. It can be inferred from these results that the reaction of AMP with OH radical can be initiated in two different ways which are hydrogen atom abstractions, hydroxyl radical addition to a benzene ring, and/or carbonyl groups [36–39].

Primary reactions

Primary degradation reaction paths are given in Scheme 1. As can be seen in Scheme 1, nine different intermediates are obtained as a result of the reactions. Among these nine reaction paths, six of them are hydrogen abstraction and three of them are hydroxyl radical addition to a benzene ring and carbonyl groups.

Electrostatic interactions of negatively charged π bonded orbitals of molecule and dipole moment of hydroxyl radical led to occur of weakly bonded complexes [38]. These weakly bonded complexes are pre-reactives. Since these structures affect the reaction barrier, they are important in the reaction mechanism [40]. These pre-reactive complexes are stabilized by the hydrogen bonds or Van der Waals attractions. They can easily be produced because their energies are lower than the reactants [41]. These pre-reactive complexes then form transition state complexes with an energy barrier to produce their primary intermediates in each of the reaction paths. The optimized structure of pre-reactive complexes, transition state complexes, and intermediate radicals are given in Figs. 2, 3, and S3 respectively. IRC plots for all of the reaction paths are given in Supplementary Information.

The energy values of all species in the primary reaction paths are given in Table S3, and the potential energy

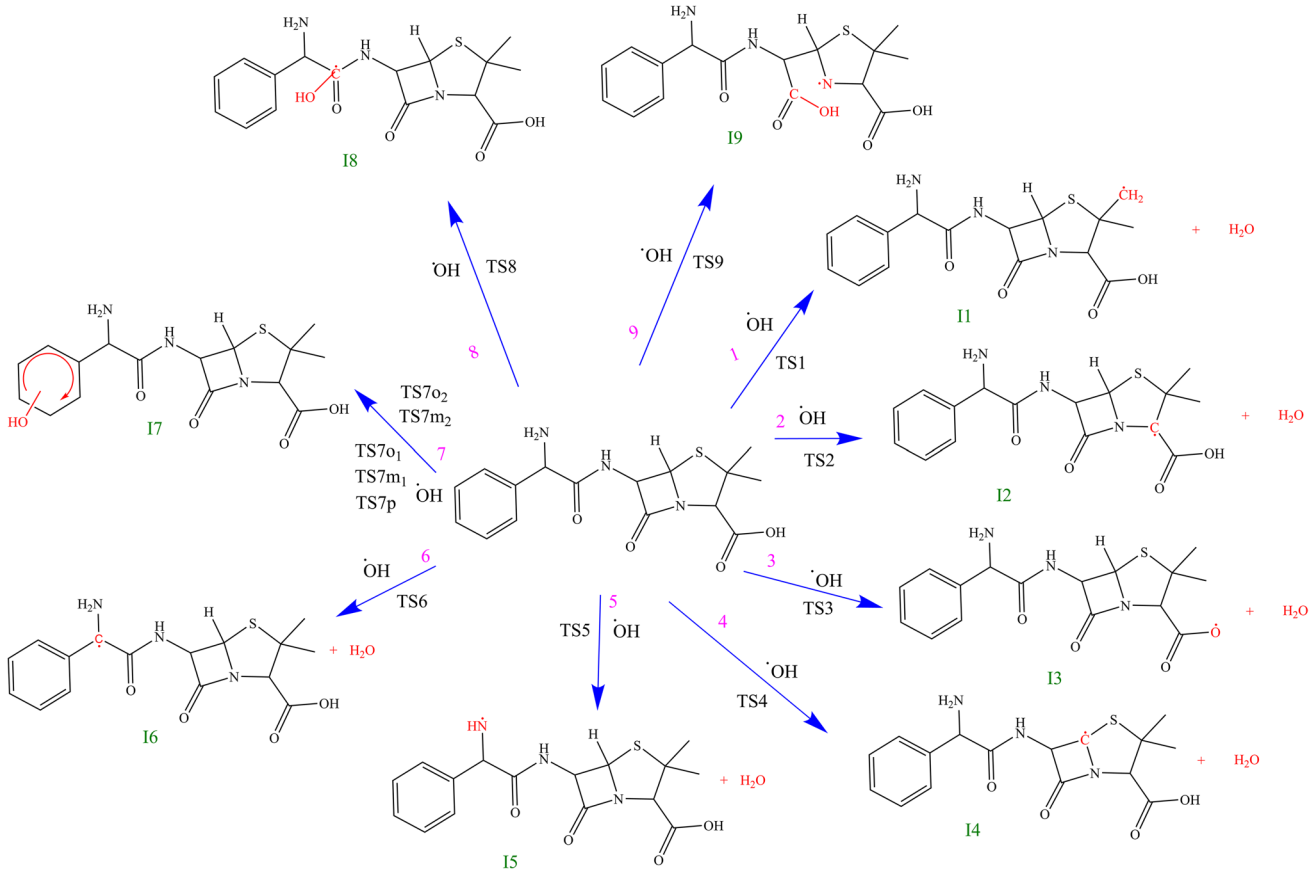

Scheme 1 Primary reaction paths for degradation

diagram for the hydrogen abstraction and hydroxyl addition reaction paths are given in Figs. 4 and S4 respectively.

Hydrogen abstraction reactions

In the hydrogen abstraction reactions, one hydrogen atom from the AMP is abstracted; water and radical intermediate are obtained. As seen from the potential energy diagram of the hydrogen abstraction reaction, at the entrance of each reaction path, formation of weakly bonded pre-reactive complexes occurs. In these reactions, the pre-reactive complexes (**PR1**–**PR6**) occur with the approaching of hydroxyl radical to the abstracted hydrogen atom with the distances of 1.64–2.82 Å. **PR1** has the longest distance of occurring hydrogen oxygen length with a value of 2.82 Å. Due to the hydrogen bonds formed in the pre-reactive complexes, their energies are lower than the reactant energies (Fig. 4). Energetically, the pre-reactive complexes' stability changes as follows: **PR6** > **PR3** > **PR4** > **PR5** > **PR2** > **PR1**.

It is understood from Fig. 4 that the distances of occurring hydrogen and oxygen bond and the breaking of hydrogen atom bonds are the sensitive measure of the transition state complexes. These transition state complexes' energies are smaller than reactant energies. In the transition state complexes (**TS1**–**TS6**), the distance between the oxygen of the hydroxyl radical and the hydrogen of the AMP molecule is 1.21 to 1.40 Å and the angle is about 99.54°. The highest value for elongation of occurring bond belongs to **TS6** (0.42 Å). The bond distance for the occurring oxygen-hydrogen bond lengths is 1.27 Å, 1.35 Å, 1.23 Å, 1.37 Å, 1.30 Å, and 1.40 Å for **TS1**–**TS6** respectively. The amount of elongation in the bonds formed in the transition state complexes is about 36.52%. The elongation in broken bonds is approximately 13.38%. The elongation in the bonds formed is higher. Thus, these results are consistent with Hammond's postulate [42], that the transition state complexes are more like reactants than products.

The activation free energies are given in Table 1. The activation free energies for hydrogen abstraction paths are found between 4.01 and 7.10 kcal mol^{-1} (Table 1). The small values of activation free energies demonstrate those reaction paths spontaneously occur in the environment. The activation free energy of **I6** is higher than other hydrogen abstraction paths, whereas the activation free energies of **I3**, **I4**, and **I5** are close to each other and lower than **I6**. According to the NBO analysis of the **I3**, **I4**, and **I5** paths, the charge of

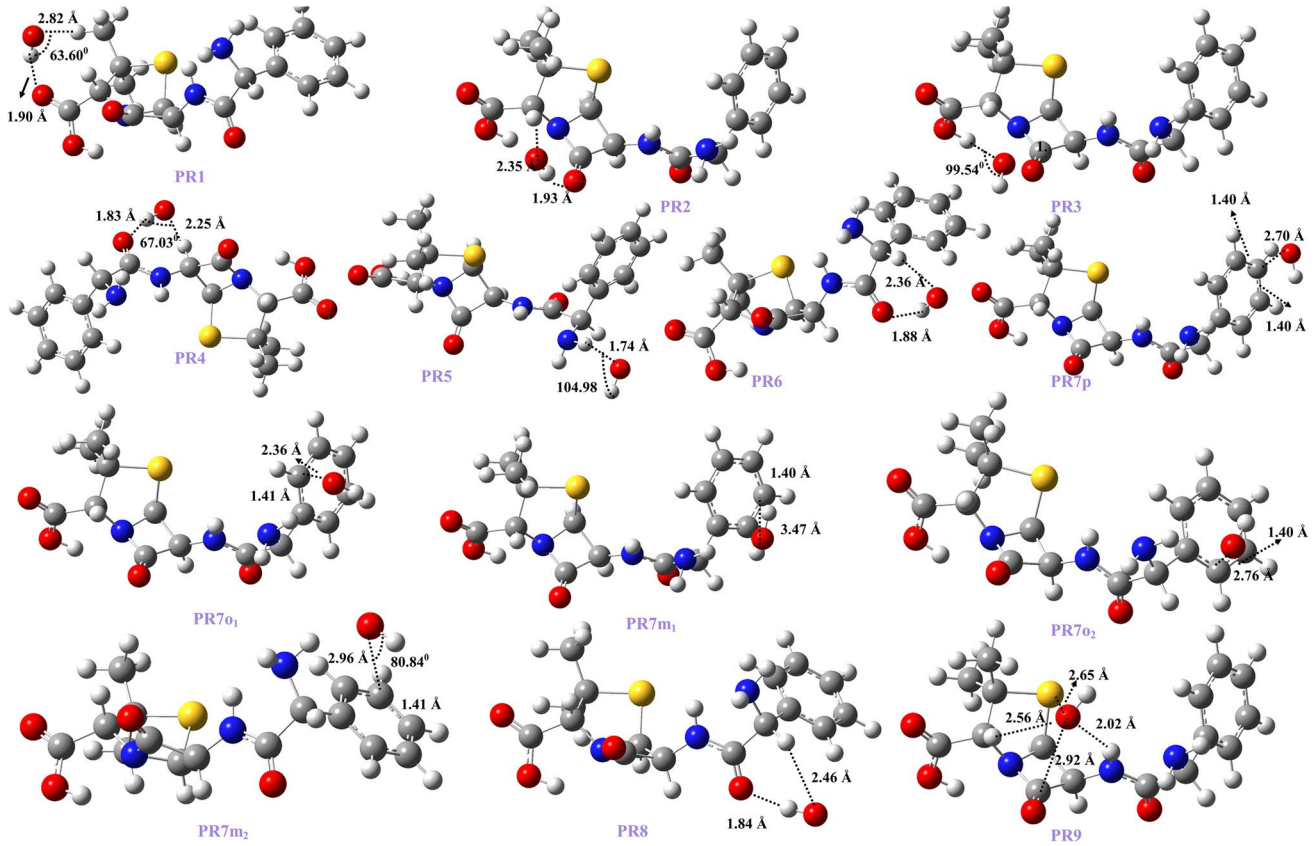

Fig. 2 Pre-reactive complexes structures

the C atom of **I4** attached to the abstracted hydrogen atom was found to be more positive than the others. So the hydrogen atom in reaction path 4 is more acidic than the others. This is compatible with the small energy of **I4**.

OH radical addition reactions

The addition reactions occur by the addition of an OH radical to the benzene ring or carbonyl groups of the AMP molecule. Pre-reactive complex geometries are given in Fig. 2. The structural changes observed in the pre-reactive complexes are around the carbon atom to which the hydroxyl radical approaches. In the **PR9** structure, a ring-like structure is formed by Van der Waals interactions as the hydroxyl radical approaches the AMP molecule. In reaction path 7, there are five different possibilities in which the OH radical can be added to the AMP molecule. These are ortho, meta, and para OH radical addition reaction paths. As it is indicated in Fig. S4, these pre-reactive complexes have smaller energies than reactants. The highest energy belongs to **PR7p** and which has also lower energy than reactants. Figure 2 shows these pre-reactive complex structures where the hydroxyl radical approaches the AMP molecule at distances ranging from 2.36 to 3.47 Å. The angle between the hydrogen atom of the hydroxyl radical and the carbon atom in the benzene ring of AMP is found to be approximately 107.81°. The angle for hydroxyl addition to carbonyl groups is greater than for benzene ring addition and is approximately 161.61°. Hydroxyl radical approaches to the carbonyl groups of AMP in **PR8** and **PR9** are almost parallel at 167.4° and 155.82° respectively. The minimum electronic energy belongs to **PR9** (Table S3; Fig. S4) which is compatible with its stabilized structure from molecular attraction forces.

The transition state structures are given in Fig. 3. The transition state formed in path 7 changes the carbon atom hybridization from sp^2 to sp^3, while the C–C bond length also varies between 0.03 and 0.04 Å. In path 7 when the hydroxyl radical approaches the benzene ring, the ring's hydrogen is directed toward the inner part of the ring. In these structures, the hydrogen atom of benzene rotates out of the benzene plane by approximately 13.18°. In paths 8 and 9, the length between the hydroxyl radical and carbon of the carbonyl group is approximately 1.77 Å. The addition of hydroxyl to a carbon atom of the carbonyl group and the breaking of the C-N bond in the beta-lactam ring occur simultaneously in path 9. As seen in Fig. S5, the electron distribution in the Single Occupied Molecular

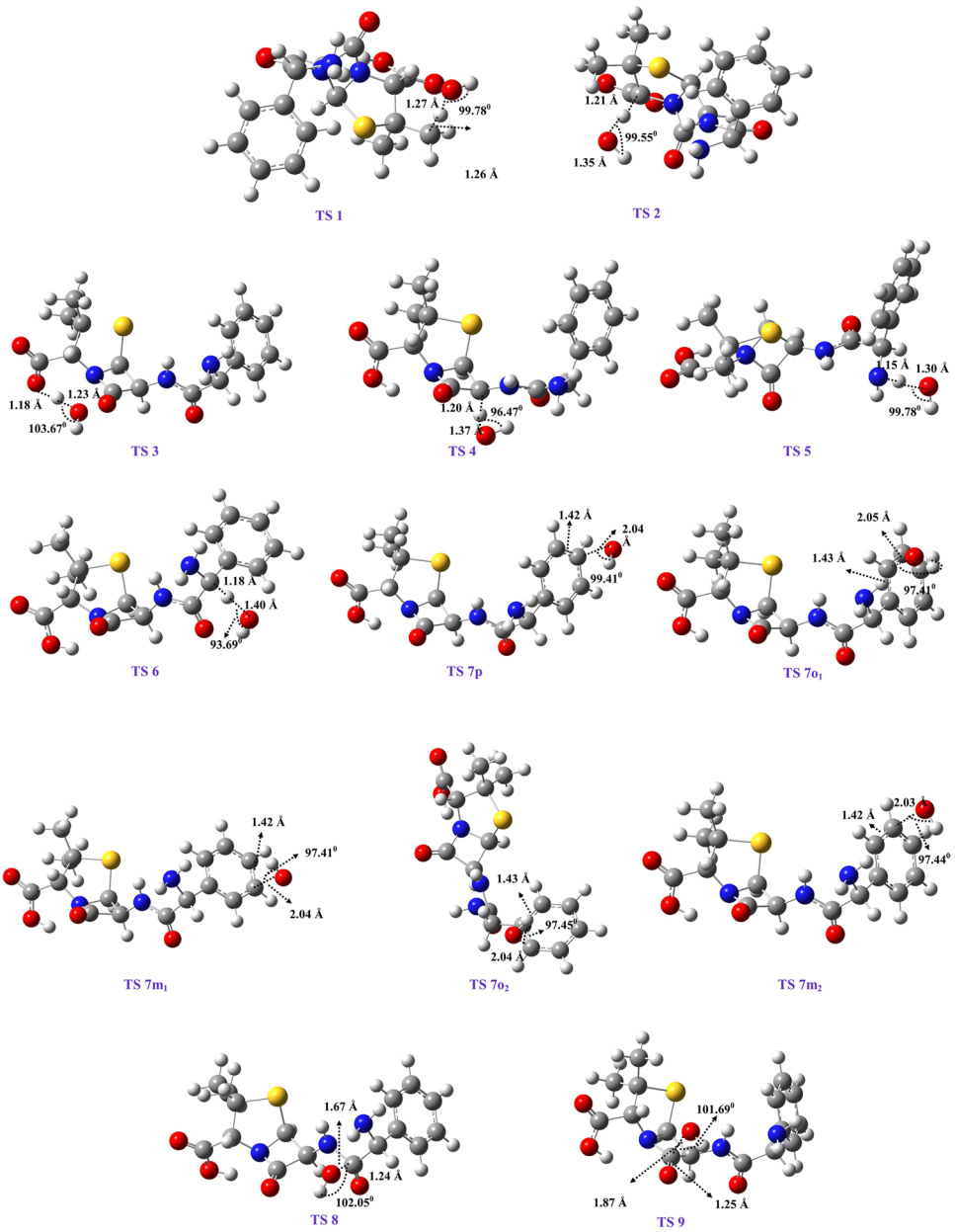

Fig. 3 Optimized structures of transition states

Orbital (SOMO) of **TS9** (reaction path 9) is in the π^* bond orbital of the carbonyl group and the p orbital of the hydroxyl radical. As shown in Fig. S4, the energies of TS8 and TS9 are higher than other transition state complexes' energies.

The activation free energies of reaction paths 7, 8, and 9 are between 2.63 and 6.20 kcal mol^{-1}. The differences in activation free energies of these reaction paths are due to the OH radical attaching different sterically hindered positions of the AMP. However, none of these activation free energy values are high enough to be studied experimentally in any of the AOP techniques [43]. The free energy values of hydroxyl radical addition to AMP are lower than hydrogen abstraction paths.

Activation free energy values of hydroxyl radical attack to the AMP molecule are lower than the hydrogen abstraction reaction paths' values. This shows that the addition of hydroxyl radical to the AMP molecule would be preferable to the reaction paths to hydrogen abstraction. The calculated results demonstrate these reaction paths proceed from the transition states with releasing of intermediate radicals for hydroxyl radical addition. The energies of intermediate radicals are lower than the reactants for all reaction paths which indicates the exothermic nature of each reaction path (Fig. S4).

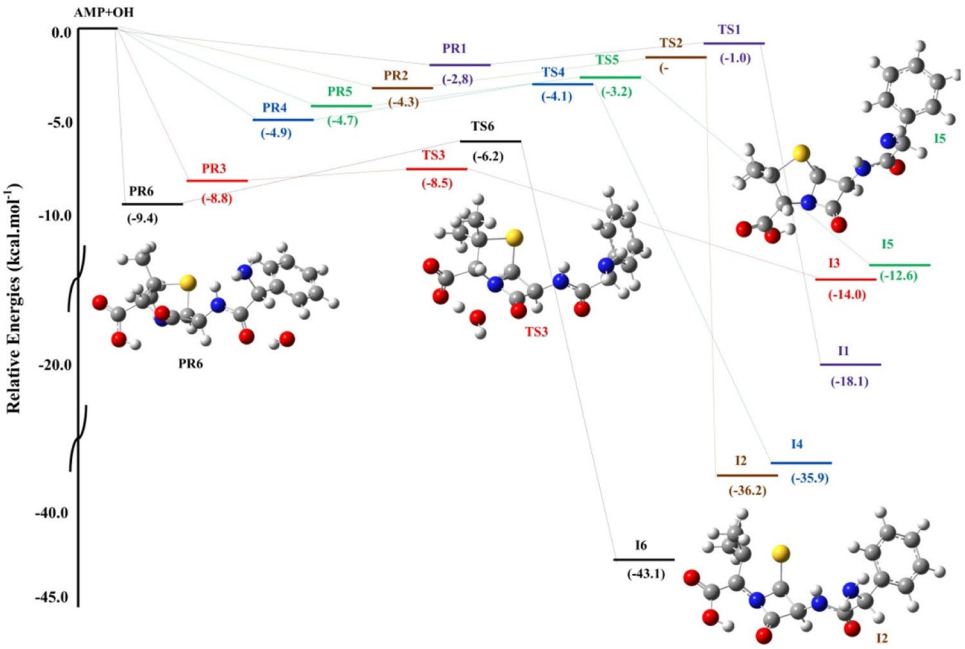

Fig. 4 Potential energy diagram for the hydrogen abstraction paths

Table 1 Enthalpy, Gibbs free energy, activation Gibbs free energy (ΔH, ΔG, $\Delta G^{\#}$, kcal mol^{-1}), imaginary frequency (I, cm^{-1}), branching ratio (f, %), and rate constants (k, M^{-1} s^{-1}) of the reaction paths

Path	ΔH	ΔG	$\Delta G^{\#}$	I	f	k
1	− 17.63	− 18.80	6.49	− 1334.09	0.079	1.08×10^{8}
2	− 35.81	− 37.05	6.12	− 924.66	0.042	5.65×10^{7}
3	− 13.58	− 15.15	4.01	− 1188.46	5.228	7.11×10^{9}
4	− 35.59	− 36.58	4.88	− 883.72	1.213	1.65×10^{9}
5	− 13.49	− 14.75	4.84	− 1138.77	1.286	1.75×10^{9}
6	− 34.31	− 34.84	7.10	− 432.50	0.029	3.91×10^{7}
7p	− 14.48	− 4.83	5.44	− 295.45	0.472	1.79×10^{8}
7o1	− 16.62	− 6.21	4.37	− 258.96	1.257	3.89×10^{9}
7m1	− 13.87	− 4.04	6.20	− 313.97	0.132	1.79×10^{8}
7o2	− 4.15	− 4.60	6.19	− 276.40	2.860	1.81×10^{8}
7m2	− 13.84	− 4.24	4.86	− 310.32	0.133	1.71×10^{9}
8	− 45.25	− 39.22	2.63	− 318.77	53.235	7.24×10^{10}
9	− 49.29	− 39.78	2.90	− 473.14	33.964	4.61×10^{10}

Energetic parameters

Kinetic and energetic parameters for all the studied reaction paths are given in Table 1. It is seen that ΔG values of the reaction paths are all negative. The Gibbs free energy and enthalpy of the reaction paths demonstrate that all reaction paths are highly exothermic and exergonic. This means that reaction paths are not only possible but also thermodynamically favoured. The absolute value of ΔG for reaction path 9 is the lowest. This indicates the formation of product **I9** is thermodynamically favoured. Compared with all reaction paths, the most stable product is also **I9** with its most negative energy value as − 1560.00 Hartree (Table S3)**.** This result is also consistent with the recent experimental results in which **I9** was determined [44–47]. The activation free energies (Table 1) for all reaction paths are very small, so they can occur immediately at room temperature. Thus, the most possible reaction path for the primary degradation reaction of AMP is found to be the addition of hydroxyl radical to the carbonyl group of the beta-lactam ring.

Rate constant and half life time

The kinetic parameters of all the reaction paths are given in Table 1. The rate constants of all paths were calculated at 298 K and 1 atm pressure. The rate constants for hydroxyl radical addition paths are higher than hydrogen abstraction paths. Thus, the hydroxyl radical addition paths are more probable than hydrogen abstraction paths. As seen in Table 1 paths 8 and 9 are the more fast reactions. The

calculated overall rate constant for the AMP + OH reaction is 1.36×10^{11} M^{-1} s^{-1}, which is slightly higher than the experimentally obtained $8.21 \times 10^{9} \pm 0.29$ M^{-1} s^{-1} [33]. The rate constants calculated using the transition state theory are higher than those found experimentally [48]. The difference between the experimental and computational rate constants may be the result of the influence of the water environment on the reaction mechanism. Water molecules have a significant effect on degradation reactions. Different solvent models can be used to solve these problems.

The relative contribution of each reaction path is needed to predict quantitatively the importance of each reaction intermediate [49]. The branching ratios of each path are obtained by dividing the rate constant of a reaction path by the overall calculated rate constant. The branching ratios of paths 1, 2, 6,7p, $7m_1$, and $7m_2$ are lower than 1%. Therefore, the contribution of these six paths to the degradation reaction is insignificant. The branching ratios of paths 8 and 9 are the highest ones with values of 53.24% and 33.96%. Thus, **I8** and **I9** are the main intermediates.

Kinetic parameters of AMP and OH radical reaction are also calculated at the temperatures of 250, 300, 350, and 400 K [50]. The rate constants for these temperatures were given in Table S4. The results of the effect of temperature on the reaction rate are given in Fig. 5. The Arrhenius formula is obtained as $lnk = 2134.2\frac{1}{T} + 19.243$. It is understood that the kinetic of the reaction of AMP with OH is negatively affected by the increasing temperature in the studied temperature range. Some studies obtained a similar result for hydroxyl radicals with organic compounds [50, 51].

The half-life time of the reaction ($t_{1/2}$) is a simple index to find the degradation feasibility and fate of an organic compound in the environment [52]. The half-life time of the studied reactions is calculated, for which the OH concentration is used in natural water as 10^{-15}–10^{-18} M [53] and is given in Fig. S6. The reaction's half-life time is varying between 2.042 h and 85.103 days. As seen in Fig. S6, when hydroxyl radical concentration decreases, $t_{1/2}$ of the degradation reaction is increased. The degradation half-life time of AMP is higher than 60 days, so it can be classified as persistent organic contaminant molecules according to Stockholm Convention on Persistent Organic Pollutants [54].

Subsequent reaction of I9

The results of the AMP + OH reactions examined above indicate that the products of the hydroxyl radical addition reactions are important for the further degradation of AMP. The structure of several different products determined by experimental methods can be explained theoretically. As previously stated, the most stable product is also **I9**. Since the mechanism of action of beta-lactam antibiotics on bacteria is the bactericidal effect of the beta-lactam ring, subsequent degradation reactions of the primary intermediate (I9) of beta-lactam ring cleavage will be discussed in this section.

The subsequent reaction scheme, reaction potential energy graph, and optimized reactive species geometries are given with Scheme 2, Figs. 6, and S7 respectively. As seen in Scheme 2, the subsequent reaction occurs with the hydroxyl radical attack on the hydrogen atom of the thiazolidine ring of **I9**. The subsequent reaction initiates the approaching of hydroxyl radical to **I9**. The distance between the oxygen atom of hydroxyl radical and to hydrogen atom of **I9** is 2.68 Å in the **PR10** structure. The **PR10** has lower energy than **I9** and OH radicals (Fig. 6). The stabilization of **PR10** depends on the hydrogen bond interaction with a distance of 1.85 Å. Then, the reaction proceeds from **PR10**

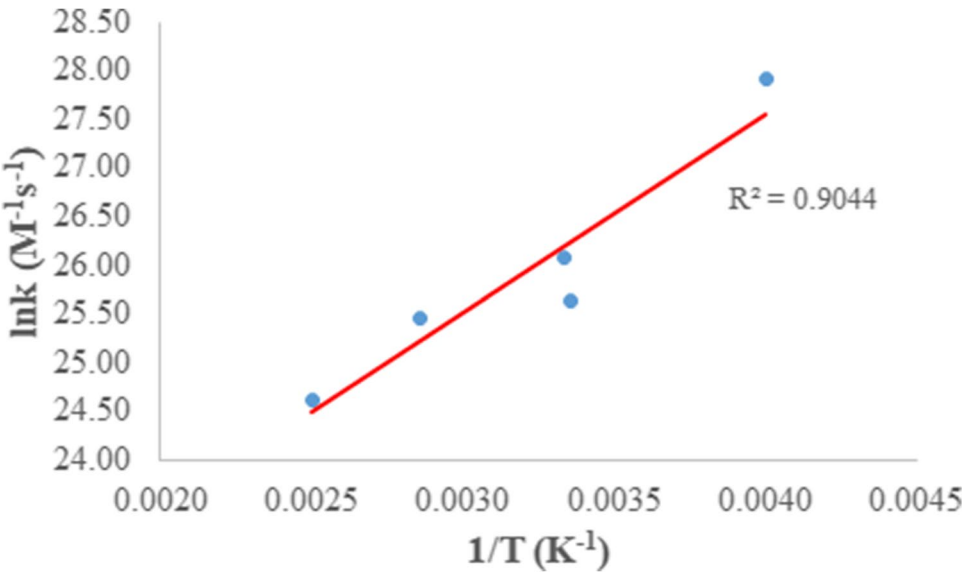

Fig. 5 The overall rate constant variation with the temperature range 250 to 400 K

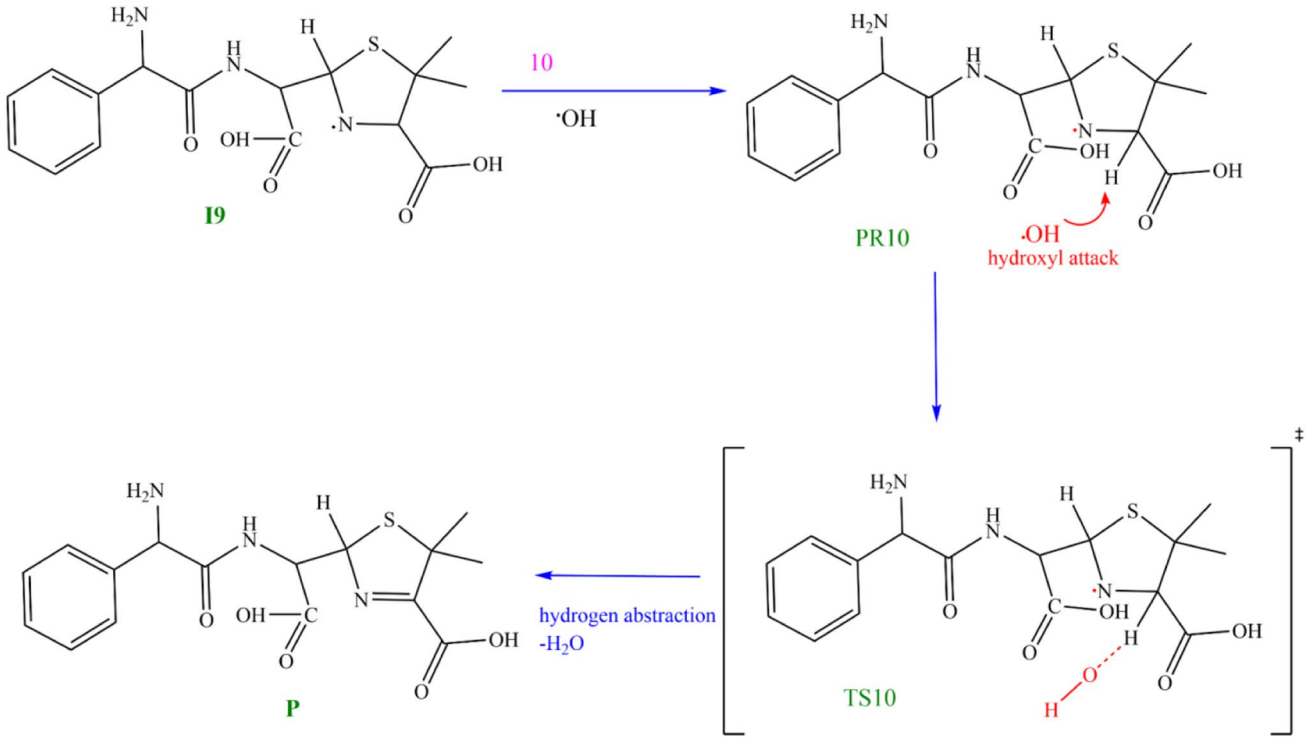

Scheme 2 Proposed mechanism for subsequent reaction

to **TS10**. The transition complex **TS10** is formed by the bond formation between the electrophilic hydroxyl radical and the nucleophilic hydrogen of **I9**.2-((2-amino-2-phenylacetamido)(carboxy)methyl)-5,5-dimethyl-2,5-dihydrothiazole-4-carboxylic acid (**P**) is obtained from this reaction via **TS10**. Belhacova et al. reported the same product in their study [12].

In **TS10**, the bond formed between the oxygen atom of the hydroxyl radical and the hydrogen atom of **I9** is 1.23 Å, while the broken bond length between carbon and hydrogen is 1.43 Å. The bond angle between the hydroxyl radical and the abstracted hydrogen atom is 68.16° (Fig. S7). The enthalpy and Gibbs free energy values of the **P** and the water molecule are – 133.93 and – 135.55 kcal mol^{-1} respectively. This reaction is exergonic, so the formation of subsequent reaction products is possible.

Toxicity evolution

AMP can be classified as a persistent organic contaminant as stated above. Especially the toxic effect of degradation intermediates in water can be considered an environmental problem due to possible toxic effects on different organisms. Therefore, we have calculated AMP and its degradation product (**P**) aquatic toxicity. The AMP acute toxicity is calculated as 160 mg L^{-1}, 172 mg L^{-1}, and 1530 mg L^{-1} for green algae, daphnid, and fish respectively. The toxicity of the subsequent product, **P**, is calculated and found 41.9 mg L^{-1}, 54.5 mg L^{-1}, and 441 mg L^{-1} for green algae, daphnid, and fish respectively. According to the Globally Harmonized System of Classification and Labelling of Chemicals (see Table S5), AMP is grouped among the most harmful chemicals. From the toxicity analysis, it appears that the toxicity values of the degradation product **P** are greater than AMP for green algae, and daphnid. The toxicity value of **P** is lower than AMP with an LC_{50} value of 441 mg L^{-1} for fish. All the above results suggest that the degradation product toxicity is higher than the parent molecule. This result supports the previous studies claiming that some degradation products of antibiotics are more toxic than the parent antibiotic [16].

Conclusion

In this study, the reaction of AMP with OH radical was modelled and the results were compared with experimental studies. The primary reactions of the AMP + OH reaction are divided into two patterns, hydrogen abstraction, and hydroxyl radical addition. The obtained major findings are given below:

1) The negative Gibbs free energy values for the primary reaction paths demonstrate that electrophilic attack of

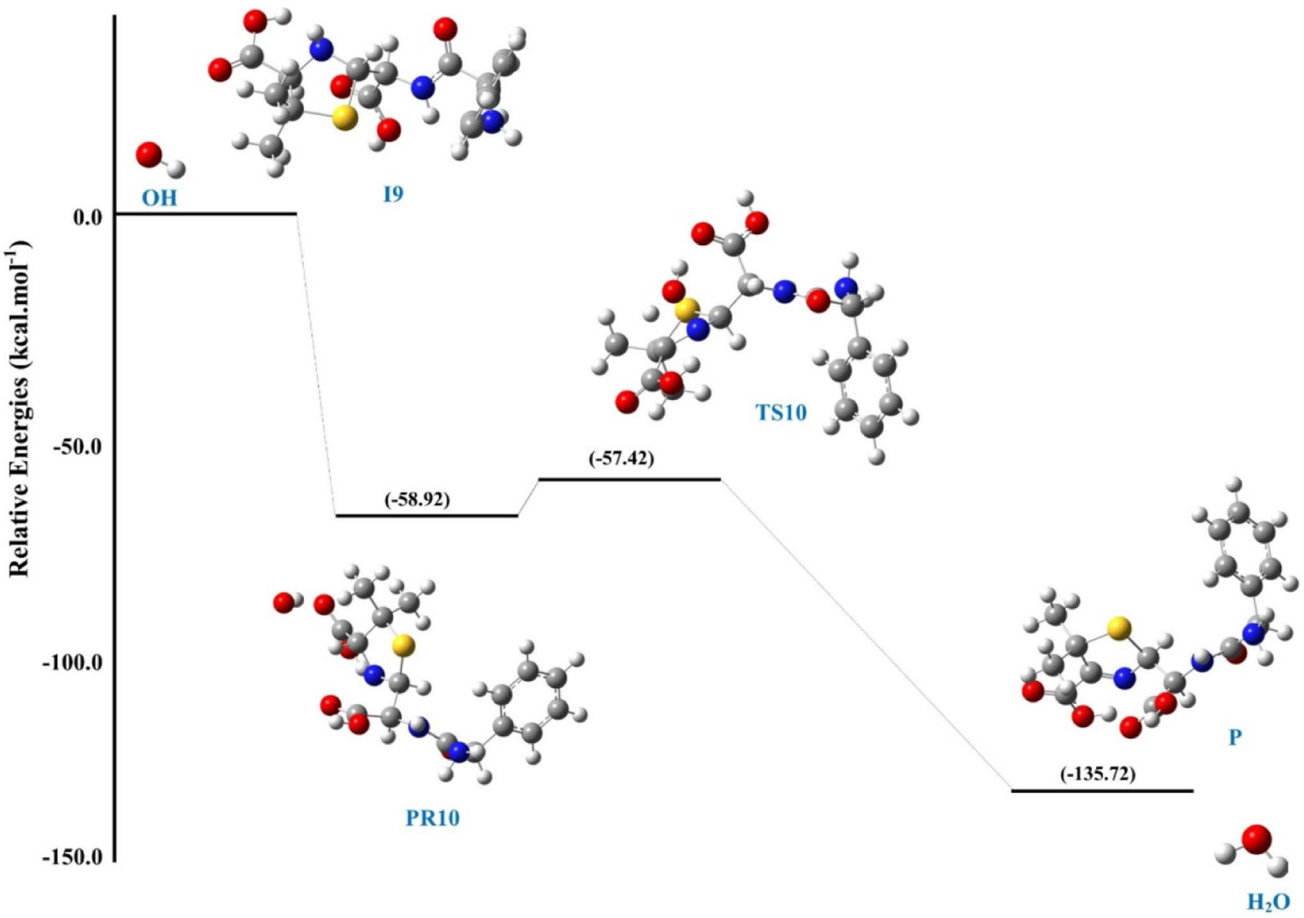

Fig. 6 Potential energy diagram for the subsequent reaction of **I9**

hydroxyl radical to AMP molecule is thermodynamically possible.

2) The activation energy of all primary reactions is lower than 20 kcal mol^{-1}, indicating that these reactions can occur easily.
3) The reaction rate constant is negatively affected by increasing temperature from 200 to 400 K. Therefore, this result may positively affect the experimental process in natural waters.
4) The branching ratio of reaction path 9 is higher than the others indicating the importance of the **I9** intermediate.
5) The half-life time of the reactions is changing between 2.042 h and 85.103 days as a function of the hydroxyl radical concentration.
6) It has been obtained from the toxicity assessment that **P** is more toxic than AMP.

Overall, it is known that numerical contaminants pass the aquatic resources from discharging of effluents. The calculation results have shown that DFT calculation can be used to explain the occurrence of experimentally obtained products, and as supplementing for further experimental studies. Thus, quantum chemical methods can be used to design suitable experimental reaction processes.

Supplementary Information The online version contains supplementary material available at https://doi.org/10.1007/s00894-023-05462-2.

Author contribution Arzu Hatipoglu: conceptualization, writing — reviewing and editing; Seyda Aydogdu: DFT calculations, writing.

Funding This study is supported by the Yildiz Technical University Research Coordination with project number FDK-2021–4138. We also received computational resources support from the Tubitak TRUBA.

Data Availability All data generated or analysed during this study are included in this published article (and its supplementary information files).

Declarations

Conflict of interest The authors declare no competing interests.

References

1. Shukla A, Khan E, Tandon P, Sinha K (2017) Study of vibrational spectra and hydrogen bonding network in dimeric and tetrameric model of ampicillin using DFT and AIM approach. J Mol Struct 1131:225–235. https://doi.org/10.1016/j.molstruc.2016.11.057
2. He X, Mezyk SP, Michael I et al (2014) Degradation kinetics and mechanism of β-lactam antibiotics by the activation of H_2O_2 and $Na_2S_2O_8$ under UV-254nm irradiation. J Hazard Mater 279:375–383. https://doi.org/10.1016/j.jhazmat.2014.07.008
3. Serna-Galvis EA, Cáceres-Peña AC, Torres-Palma RA (2020) Elimination of representative fluoroquinolones, penicillins, and cephalosporins by solar photo-Fenton: degradation routes, primary transformations, degradation improvement by citric acid addition, and antimicrobial activity evolution. Environ Sci Pollut Res 27:41381–41393. https://doi.org/10.1007/s11356-020-10069-8
4. Xu L, Li W, Désesquelles P et al (2019) A statistical model and DFT study of the fragmentation mechanisms of metronidazole by advanced oxidation processes. J Phys Chem A 123:933–942. https://doi.org/10.1021/acs.jpca.8b10554
5. Ioannou-Ttofa L, Raj S, Prakash H, Fatta-Kassinos D (2019) Solar photo-Fenton oxidation for the removal of ampicillin, total cultivable and resistant E. coli and ecotoxicity from secondary-treated wastewater effluents. Chem Eng J 355:91–102. https://doi.org/10.1016/j.cej.2018.08.057
6. Darwish M, Mohammadi A, Assi N (2016) Integration of nickel doping with loading on graphene for enhanced adsorptive and catalytic properties of CdS nanoparticles towards visible light degradation of some antibiotics. J Hazard Mater 320:304–314. https://doi.org/10.1016/j.jhazmat.2016.08.043
7. Rozas O, Contreras D, Mondaca MA et al (2010) Experimental design of Fenton and photo-Fenton reactions for the treatment of ampicillin solutions. J Hazard Mater 177:1025–1030. https://doi.org/10.1016/j.jhazmat.2010.01.023
8. Sharma VK, Liu F, Tolan S et al (2013) Oxidation of β-lactam antibiotics by ferrate(VI). Chem Eng J 221:446–451. https://doi.org/10.1016/j.cej.2013.02.024
9. Shukla A, Khan E, Srivastava A et al (2016) A computational study on molecular structure, multiple interactions, chemical reactivity and molecular docking studies on 6[D (−) α-amino-phenylacetamido] penicillanic acid (ampicillin). Mol Simul 42:863–873. https://doi.org/10.1080/08927022.2015.1089996
10. Vidal J, Huiliñir C, Santander R et al (2019) Degradation of ampicillin antibiotic by electrochemical processes: evaluation of antimicrobial activity of treated water. Environ Sci Pollut Res 26:4404–4414. https://doi.org/10.1007/s11356-018-2234-5
11. Serna-Galvis EA, Montoya-Rodríguez D, Isaza-Pineda L et al (2019) Sonochemical degradation of antibiotics from representative classes—considerations on structural effects, initial transformation products, antimicrobial activity and matrix. Ultrason Sonochem 50:157–165. https://doi.org/10.1016/j.ultsonch.2018.09.012
12. Belhacova L, Bibova H, Marikova T et al (2021) Removal of ampicillin by heterogeneous photocatalysis: combined experimental and dft study. Nanomaterials 11. https://doi.org/10.3390/nano11081992
13. Timm A, Borowska E, Majewsky M et al (2019) Photolysis of four β-lactam antibiotics under simulated environmental conditions: degradation, transformation products and antibacterial activity. Sci Total Environ 651:1605–1612. https://doi.org/10.1016/j.scitotenv.2018.09.248
14. Yabalak E (2018) An approach to apply eco-friendly subcritical water oxidation method in the mineralization of the antibiotic ampicillin. J Environ Chem Eng 6:7132–7137. https://doi.org/10.1016/j.jece.2018.10.010
15. Li T, Xu X, Fu S et al (2014) Structural elucidation of stress degradation products of ampicillin sodium by liquid chromatography/hybrid triple quadrupole linear ion trap mass spectrometry and liquid chromatography/hybrid quadrupole time-of-flight mass spectrometry. Rapid Commun Mass Spectrom 28:1929–1936. https://doi.org/10.1002/rcm.6970
16. Ribeiro AR, Sures B, Schmidt TC (2018) Cephalosporin antibiotics in the aquatic environment: a critical review of occurrence, fate, ecotoxicity and removal technologies. Environ Pollut 241:1153–1166
17. Elmolla ES, Chaudhuri M (2010) Photocatalytic degradation of amoxicillin, ampicillin and cloxacillin antibiotics in aqueous solution using UV/TiO2 and UV/H2O2/TiO2 photocatalysis. Desalination 252:46–52. https://doi.org/10.1016/j.desal.2009.11.003
18. Szabó L, Tóth T, Engelhardt T et al (2016) Change in hydrophilicity of penicillins during advanced oxidation by radiolytically generated OH compromises the elimination of selective pressure on bacterial strains. Sci Total Environ 551–552:393–403. https://doi.org/10.1016/j.scitotenv.2016.02.002
19. Yao J, Tang Y, Zhang Y et al (2022) New theoretical investigation of mechanism, kinetics, and toxicity in the degradation of dimetridazole and ornidazole by hydroxyl radicals in aqueous phase. J Hazard Mater 422. https://doi.org/10.1016/j.jhazmat.2021.126930
20. Xu M, Yan S, Sun S et al (2022) N, N -diethyl-m-toluamide (DEET) degradation by •oH and SO4•--assisted AOPs in wastewater treatment: theoretical studies into mechanisms, kinetics and toxicity. J Environ Chem Eng 10. https://doi.org/10.1016/j.jece.2022.108435
21. Xu M, Yao J, Sun S et al (2021) Theoretical calculation on the reaction mechanisms, kinetics and toxicity of acetaminophen degradation initiated by hydroxyl and sulfate radicals in the aqueous phase. Toxics 9. https://doi.org/10.3390/toxics9100234
22. Frisch MJ, Trucks GW, Schlegel HB, Scuseria GE, Robb MA, Cheeseman JR, Scalmani G, Barone V, Petersson GA, Nakatsuji H, Li X, Caricato M, Marenich AV, Bloino J, Janesko BG, Gomperts R, Mennucci B, Hratchian HP, Ortiz JV, Izmaylov AF, Sonnenberg JL, Williams-Young D, Ding F, Lipparini F, Egidi F, Goings J, Peng B, Petrone A, Henderson T, Ranasinghe D, Zakrzewski VG, Gao J, Rega N, Zheng G, Liang W, Hada M, Ehara M, Toyota K, Fukuda R, Hasegawa J, Ishida M, Nakajima T, Honda Y, Kitao O, Nakai H, Vreven T, Throssell K, Montgomery JA, Peralta Jr. JE, Ogliaro F, Bearpark MJ, Heyd JJ, Brothers EN, Kudin KN, Staroverov VN, Keith TA, Kobayashi R, Normand J, Raghavachari K, Rendell AP, Burant JC, Iyengar SS, Tomasi J, Cossi M, Millam JM, Klene M, Adamo C, Cammi R, Ochterski JW, Martin RL, Morokuma K, Farkas O, Foresman JB, Fox DJ (2016) Gaussian 16, Revision C.01 Gaussian, Inc., Wallingford
23. Gonzalez C, Schlegel HB (1990) Reaction path following in mass-weighted internal coordinates Cartesians and with internal coordinates without mass-weighting. J Phys Chem 94:5523. https://doi.org/10.1021/j100377a021
24. Foresman J, Frish E (1996) Exploring chemistry. Gaussian Inc, Pittsburg
25. Dennington R, Keith TA, Millam JM (2016) GaussView, Version 5.0. Semichem Inc., Shawnee Mission, KS
26. Saïd AE hadj, Mekelleche SM (2021) Antioxidant activity of Trolox derivatives toward methylperoxyl radicals: thermodynamic and kinetic theoretical study. Theor Chem Acc 140. https://doi.org/10.1007/s00214-021-02815-z
27. Levine IN (2009) Physical Chemistry, 6th edn. Mc Graw Hill Higher Education, New York
28. Yang J, Lv G, Li T et al (2022) Theoretical insight into the degradation of diclofenac by hydroxyl and sulfate radicals in

aqueous-phase: Mechanisms, kinetics and eco-toxicity. J Environ Chem Eng 10. https://doi.org/10.1016/j.jece.2022.108311
29. Sanches-Neto FO, Ramos B, Lastre-Acosta AM et al (2021) Aqueous picloram degradation by hydroxyl radicals: unveiling mechanism, kinetics, and ecotoxicity through experimental and theoretical approaches. Chemosphere 278. https://doi.org/10.1016/j.chemosphere.2021.130401
30. Milenković DA, Dimić DS, Avdović EH et al (2020) Advanced oxidation process of coumarins by hydroxyl radical: towards the new mechanism leading to less toxic products. Chem Eng J 395. https://doi.org/10.1016/j.cej.2020.124971
31. Tay KS, Madehi N (2015) Ozonation of ofloxacin in water: by-products, degradation pathway and ecotoxicity assessment. Sci Total Environ 520:23–31. https://doi.org/10.1016/j.scitotenv.2015.03.033
32. Bekbolet M, Çinar Z, Kiliç M et al (2009) Photocatalytic oxidation of dinitronaphthalenes: theory and experiment. Chemosphere 75:1008–1014. https://doi.org/10.1016/j.chemosphere.2009.01.051
33. Dail MK, Mezyk SP (2010) Hydroxyl-radical-induced degradative oxidation of β-lactam antibiotics in water: absolute rate constant measurements. J Phys Chem A 114:8391–8395. https://doi.org/10.1021/jp104509t
34. Antonin VS, Aquino JM, Silva BF et al (2019) Comparative study on the degradation of cephalexin by four electrochemical advanced oxidation processes: evolution of oxidation intermediates and antimicrobial activity. Chem Eng J 372:1104–1112. https://doi.org/10.1016/j.cej.2019.04.185
35. Song W, Chen W, Cooper WJ et al (2008) Free-radical destruction of β-lactam antibiotics in aqueous solution. J Phys Chem A 112:7411–7417. https://doi.org/10.1021/jp803229a
36. Vione D, de Laurentiis E, Berto S et al (2016) Modeling the photochemical transformation of nitrobenzene under conditions relevant to sunlit surface waters: reaction pathways and formation of intermediates. Chemosphere 145:277–283. https://doi.org/10.1016/j.chemosphere.2015.11.039
37. Kovacevic G, Sabljic A (2013) Theoretical study on the mechanism and kinetics of addition of hydroxyl radicals to fluorobenzene. J Comput Chem 34:646–655. https://doi.org/10.1002/jcc.23175
38. Kovacevic G, Sabljic A (2013) Mechanisms and reaction-path dynamics of hydroxyl radical reactions with aromatic hydrocarbons: the case of chlorobenzene. Chemosphere 92:851–856. https://doi.org/10.1016/j.chemosphere.2013.04.041
39. Li C, Zheng S, Chen J et al (2018) Kinetics and mechanism of [rad]OH-initiated atmospheric oxidation of organophosphorus plasticizers: a computational study on tri-p-cresyl phosphate. Chemosphere 201:557–563. https://doi.org/10.1016/j.chemosphere.2018.03.034
40. Hatipoglu A, Vione D, Yalçin Y et al (2010) Photo-oxidative degradation of toluene in aqueous media by hydroxyl radicals. J Photochem Photobiol A Chem 215:59–68. https://doi.org/10.1016/j.jphotochem.2010.07.021
41. Aydogdu S, Hatipoglu A, Eren B, Gurkan YY (2021) Photodegradation kinetics of organophosphorous with hydroxyl radicals: experimental and theoretical study. J Serb Chem Soc 86:955–969. https://doi.org/10.2298/JSC210409056A
42. Hammond GS (1955) A correlation of reaction rates. J Am Chem Soc 77:334–338. https://doi.org/10.1021/ja01607a027
43. Xia H, Zhang W, Yang Y et al (2021) Degradation mechanism of tris(2-chloroethyl) phosphate (TCEP) as an emerging contaminant in advanced oxidation processes: A DFT modelling approach. Chemosphere 273. https://doi.org/10.1016/j.chemosphere.2021.129674
44. Guo Y, Tsang DCW, Zhang X, Yang X (2018) Cu(II)-catalyzed degradation of ampicillin: effect of pH and dissolved oxygen. Environ Sci Pollut Res 25:4279–4288. https://doi.org/10.1007/s11356-017-0524-y
45. Sohrabi A, Haghighat G, Shaibani PM et al (2019) Degradation of pharmaceutical contaminants in water by an advanced plasma treatment. Desalination Water Treat 139:202–221. https://doi.org/10.5004/dwt.2019.23297
46. Mirzaei A, Haghighat F, Chen Z, Yerushalmi L (2019) Sonocatalytic removal of ampicillin by Zn(OH)F: effect of operating parameters, toxicological evaluation and by-products identification. J Hazard Mater 375:86–95. https://doi.org/10.1016/j.jhazmat.2019.04.069
47. Peterson JW, Petrasky LJ, Seymour MD et al (2012) Adsorption and breakdown of penicillin antibiotic in the presence of titanium oxide nanoparticles in water. Chemosphere 87:911–917. https://doi.org/10.1016/j.chemosphere.2012.01.044
48. Zhao Y, Truhlar DG (2008) The M06 suite of density functionals for main group thermochemistry, thermochemical kinetics, noncovalent interactions, excited states, and transition elements: Two new functionals and systematic testing of four M06-class functionals and 12 other functionals. Theor Chem Acc 120:215–241. https://doi.org/10.1007/s00214-007-0310-x
49. Gao Y, Ji Y, Li G, An T (2014) Mechanism, kinetics and toxicity assessment of OH-initiated transformation of triclosan in aquatic environments. Water Res 49:360–370. https://doi.org/10.1016/j.watres.2013.10.027
50. Gour NK, Borthakur K, Paul S, Chandra Deka R (2020) Tropospheric degradation of 2-fluoropropene (CH3CF[dbnd]CH2) initiated by hydroxyl radical: reaction mechanisms, kinetics and atmospheric implications from DFT study. Chemosphere 238. https://doi.org/10.1016/j.chemosphere.2019.124556
51. Arathala P, Musah RA (2020) Computational study investigating the atmospheric oxidation mechanism and kinetics of dipropyl thiosulfinate initiated by OH radicals and the fate of propanethiyl radical. J Phys Chem A 124:8292–8304. https://doi.org/10.1021/acs.jpca.0c05200
52. Gao Y, An T, Fang H et al (2014) Computational consideration on advanced oxidation degradation of phenolic preservative, methylparaben, in water: mechanisms, kinetics, and toxicity assessments. J Hazard Mater 278:417–425. https://doi.org/10.1016/j.jhazmat.2014.05.081
53. Burns JM, Cooper WJ, Ferry JL et al (2012) Methods for reactive oxygen species (ROS) detection in aqueous environments. Aquat Sci 74:683–734. https://doi.org/10.1007/s00027-012-0251-x
54. Klasmeier J, Matthies M, Macleod M et al (2006) Application of multimedia models for screening assessment of long-range transport potential and overall persistence. Environ Sci Technol 40:53–60. https://doi.org/10.1021/es0512024